Mathematical Biosciences and Engineering

MBE, 18(1): 800–816.
DOI: 10.3934/mbe.2021042
Received: 23 October 2020
Accepted: 11 December 2020
Published: 22 December 2020

http://www.aimspress.com/journal/MBE

Research article

Thoracic aorta stent grafts design in terms of biomechanical investigations into flexibility

Zongchao Liu[1], Linhui Wu[1], Junwei Yang[1], Fangsen Cui[2], Pei Ho[3], Liping Wang[4], Jianghui Dong[4,*] and Gongfa Chen[1,*]

[1] School of Civil and Transportation Engineering, Guangdong University of Technology, Guangzhou 510006, China
[2] Institute of High Performance Computing (IHPC), Agency for Science, Technology and Research (A*STAR), Singapore 138632, Singapore
[3] Department of Cardiac, Thoracic & Vascular Surgery, National University Health System, Singapore 119228, Singapore
[4] UniSA Clinical & Health Sciences, University of South Australia, Adelaide SA 5001, Australia

* **Correspondence:** Email: jianghui.dong@mymail.unisa.edu.au, gongfa.chen@gdut.edu.cn; Tel: +8613662483527, (618)83022715; Fax: (618)83021087.

Abstract: The present study aimed to design and optimize thoracic aorta stent grafts (SGs) based on the influence of geometric parameters on flexibility and durability. Five geometric parameters were selected, including strut height, strut number, strut radius, wire diameter, and graft thickness. Subsequently, 16 finite element (FE) models were established with an orthogonal design consisting of five factors and four levels. The influences of a single factor and all the geometric parameters' influence magnitude on the device flexibility were then determined. The results showed that all the other parameters had an opposite effect on global and local flexibility except for the wire diameter. The graft thickness exhibited the most remarkable impact on the global flexibility of SGs, while the strut radius influenced flexibility slightly. However, for the local flexibility analysis, the graft thickness became the least significant factor, and the wire diameter exerted the most significant influence. The SG with better global flexibility can be guided easily in the tortuous vessels, and better local flexibility improves the sealing effect between the graft and aortic arch. In conclusion, this study's results indicated that these geometric parameters exerted different influences on flexibility and durability, providing a strategy for designing thoracic aorta SGs, especially for the thoracic aortic arch diseases.

Keywords: finite element method; flexibility; geometric parameters; orthogonal test; thoracic aorta

1. Introduction

Thoracic endovascular aortic repair (TEVAR) is a minimally invasive procedure for the aortic arch diseases; it reduces the operative morbidity and mortality compared with the traditional open surgical repair procedure [1–3]. However, the procedure mainly benefits descending aorta diseases. It still remains significant challenges for the aortic arch diseases due to the complex morphological structures and severely tortuous aortic arch [4]. Maintaining the blood perfusion in branches and good sealing effect are the priorities for the application of TEVAR at the aortic arch [5]. More recently, a hybrid operative procedure and chimney graft technique have been proposed to preserve aortic lateral branches' perfusion [6,7]. However, an inadequate seal between the SGs and the vessel is still a challenging problem.

Flexibility is one of the critical features of an SG for clinical applications [8] and determines the SG's ability to fit the vessels [9]. If the flexibility is insufficient, the SG will be easily twisted when guided through tortuous arteries, causing complications [10–13]. On the contrary, good flexibility enables the expanded stent to follow the vessel's contour and reduce distortion at the stent–vessel interface [12]. Accordingly, improved flexibility will extend the application of stents in a wide range of anatomical vascular morphology [13,14]. Endoleaks might exist if the expanded device does not adapt to the artery properly due to the lack of flexibility [15–17]. Therefore, the improved flexibility of SGs can also enhance the sealing effect, minimizing endoleak, and other complication risks [2].

Numerical methods have been applied in investigating the biomechanical behaviors of SGs for the low-cost compared with experimental tests [18–20]. Complex biomechanical environments can be ideally simulated *in vivo* and *in vitro* to assess the device performance [21–23]. Flexibility is a crucial performance of SGs in EVAR, with a close relationship with complications [2,24]. The stent flexibility is influenced significantly by the design of SGs. Spiral and circular stents are more flexible than the Z-shaped ones [12,15]. Stent structures also affect the device flexibility at both expanded and unexpanded states [9,14]. The wire rings connected by the point symmetrical links can improve stent flexibility [25]. The multi-linked stent possessed the best longitudinal flexibility, and the crown stent was the stiffest in a series of slotted tube designs [12]. Apart from the shape and structure of SGs, other geometric parameters also influence flexibility. A larger strut radius and smaller strut width can make the stent more flexible [26–28]. A decrease in flexibility of braided monofilament stent with increased wire diameter and strut number has also been confirmed [29]. In addition, the graft properties also influence the device directly; a highly flexible stent has been developed, assembled with ultra-thin silicone covering [30]. These mainly concentrate at the abdominal aorta or the carotid artery SGs; very few studies have focused on the thoracic aorta SGs. The geometric parameters' influential degrees on the SG flexibility have not been studied yet. On the other hand, factors or even one single factor have partially been investigated; however, the major influences of geometric parameters on the device flexibility are not clear yet. The durability of SGs induced by both the stent and fabric fracture should be focused on during the analyses. Fabric tear might be more frequent with Z-shaped SGs. Although it is very rare in the clinical reports about the fabric tear [11,31], complications induced by the fabric tear have been reported [32]. However, the durability of SGs influenced by the geometrical parameters has not been studied.

Therefore, this work aimed to investigate the thoracic aorta SGs in terms of the influence of geometric parameters on flexibility and durability via FE analyses. First, 16 FE models were established with an orthogonal design with five factors and four levels. Then, the influences of a single factor and the geometric parameters' influences on the device flexibility were determined. Lastly, SGs' structural durability during bending was estimated. The influence of the parameters was also examined in the design process.

2. Materials and methods

FEA can be used to carry out repeated tests with a lower cost, find the most vulnerable point in the model, and optimize it. As one of its merits, the FEA can simulate the effect before surgery, which cannot be tried in clinical practice. The finite element models of stent-grafts with different geometrical parameters can be modeled easily and quickly and can be used to reveal the stress and strain distributions of each position.

2.1. Geometry of commercial SG and modeling

A commercially available thoracic aorta SG (Lifetech, Shenzhen, Guangdong Province, China) was selected as the basic design in the current study (Figures 1 and 2). The SG consists of six Type I rings near the distal end, four Type II rings located in the middle of the SG, and one Type III ring that closes to the right of Type II rings. The detailed dimensions of the ring Types are summarized and presented in Table 1 and Figure 3. In addition, one ring that contains twelve struts measuring 7 mm in height and one bell-shaped ring is set at the proximal end to improve the anchoring ability of SG within the vessels. In the commercial SG, all the struts have a radius of 1.2 mm, and all the metal wires have a wire diameter of 0.55 mm. All the rings are soldered to the lateral bars (Figure 1b). In the FE model, there are three Type I rings, four Type II rings, and one Type III ring. All the rings were connected by the straight lateral bar. The bare metal stent was fully covered with an 0.1-mm-thick and 150-mm-long graft (Figure 2c). The 3D geometric model was established in Solidworks (Dassault Systems Corp, Massachusetts, USA).

Table 1. The details of the ring types.

Ring type	Ring number	Strut number (each ring)	Strut height (mm)	Strut radius (mm)
Type I	3	7	15	1.2
Type II	4	4, 5	14, 9	1.2
Type III	1	9	12	1.2

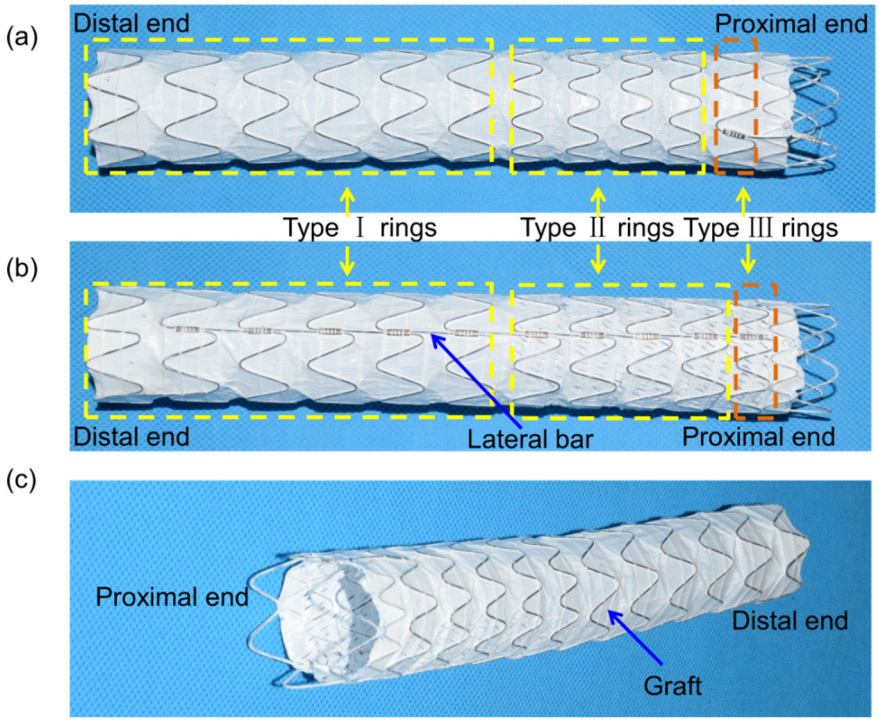

Figure 1. The geometry of the available commercial SG; (a) the side without a lateral bar; (b) the side with a lateral bar; and (c) isometric view.

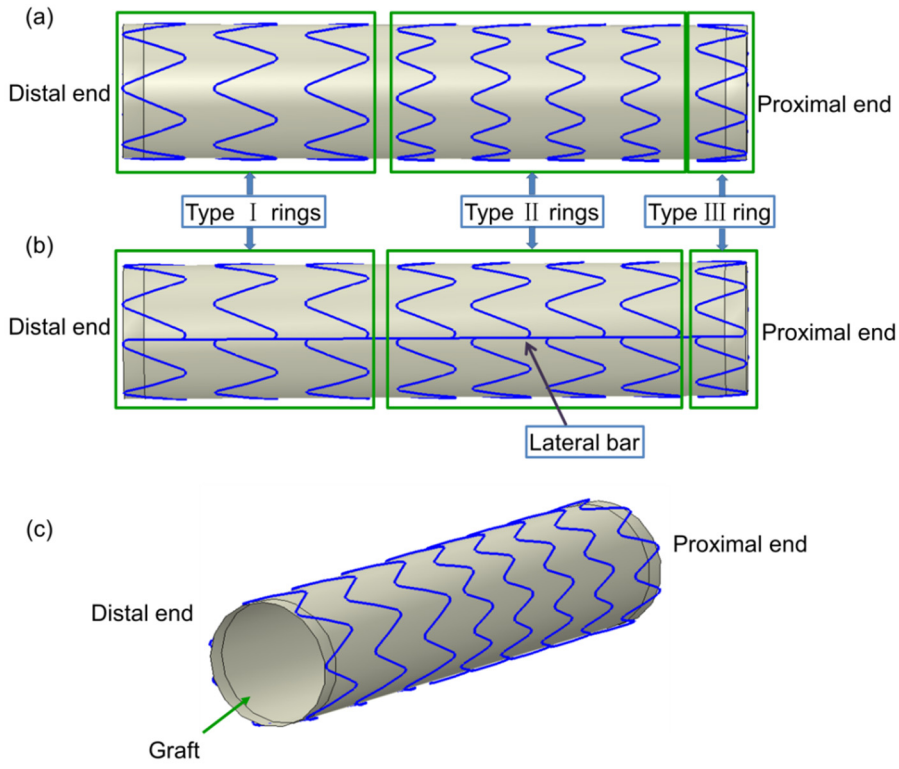

Figure 2. Finite element (FE) model; (a) the side without a lateral bar; (b) the side with a lateral bar; and (c) isometric view.

2.2. Orthogonal design

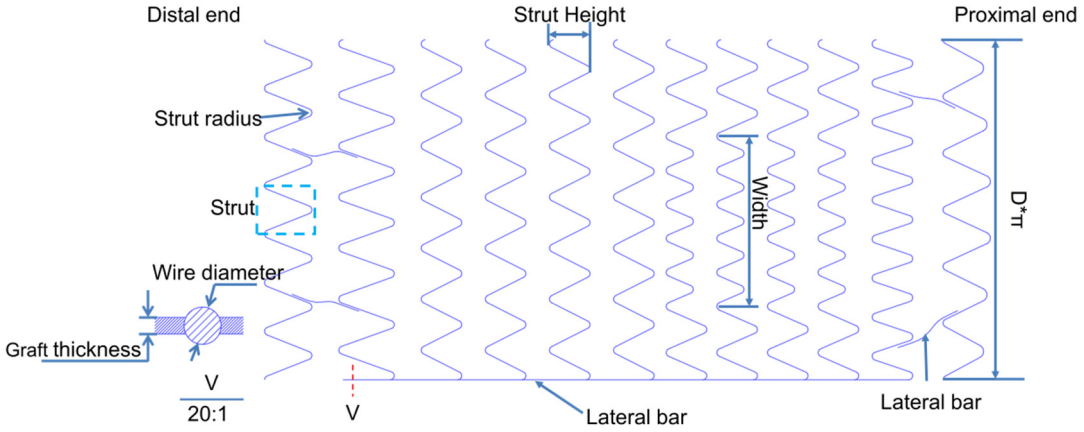

Figure 3. The variable parameters.

Most of the previous stent flexibility studies have focused on the influence of single or double factors [9,28,29]. The influence of multiple factors has rarely been studied, and the important ranking of the parameters has not been investigated. In this study, five geometric parameters, including four from the bare stent (strut height, strut number, strut radius, and wire diameter) and one from the graft (thickness), were investigated in terms of SG flexibility and durability at the same time (Figure 3). Orthogonal analysis of five factors and four levels was designed to determine the effects of geometric parameters on SG's performance simultaneously, using an efficient and inexpensive method. Hence, 16 specimens were analyzed. Table 2 lists the geometric features of every specimen. Specimen 1 (sp1) was defined as the original model. A to E represent the geometric parameters in terms of strut height, strut number, strut radius, wire diameter, and graft thickness, marked in Figure 3. The numbers 1 to 4 denote the factor levels. Since the strut height and strut number in the three types of the rings were different, the calculations would increase enormously if the real heights and strut numbers of every ring type were defined as the factors. Therefore, factors A and B of all the rings were described by their variation (Delta value) compared with the original model (Table 3). For instance, the 2nd level value of factor A meant that all the strut heights were 2 mm shorter than sp1. The 2nd level of factor B meant that there were two fewer struts in all the rings than sp1. Table 2 summarizes the values of A_i to E_i (i = 1, 2, 3, 4). For example, compared with sp1, sp8 has two fewer struts in each ring, and its ring strut height is 2 mm shorter. Besides, sp8 had a strut radius of 0.8 mm, a wire diameter of 0.65 mm, and was covered with an 0.1 mm-thick graft.

The maximum reaction moment (RM), the spacing variation of the Type II rings, and both the circumferential strain (CS) and longitudinal strain (LS) in all the specimens can be obtained after the analyses are completed. The K_i (i = 1, 2, 3, 4) in the orthogonal table is used to analyze each factor's effect. They are calculated by summing the values obtained from the same factor under the same level i among all the models. For instance, when K_{B1} is used to analyze the influence on factor B's global flexibility under the 1st level, it is calculated by summing up the RMs obtained in sp1, sp5, sp9, and sp13. After confirming all the K_i values, R can be used to reflect all the factors' influence degree, where R is obtained from the difference of the maximum and minimum K_i. A higher R-value means that the factor has a more remarkable influence on the flexibility or durability.

Table 2. Orthogonal design table.

Specimen number	Factors					Performances			
	A	B	C	D	E	Global flexibility	Local flexibility	Durability	
1	1	1	1	1	1	RM	SV	LS	CS
2	1	2	2	2	2	RM	SV	LS	CS
3	1	3	3	3	3	RM	SV	LS	CS
4	1	4	4	4	4	RM	SV	LS	CS
5	2	1	2	3	4	RM	SV	LS	CS
6	2	2	1	4	3	RM	SV	LS	CS
7	2	3	4	1	2	RM	SV	LS	CS
8	2	4	3	2	1	RM	SV	LS	CS
9	3	1	3	4	2	RM	SV	LS	CS
10	3	2	4	3	1	RM	SV	LS	CS
11	3	3	1	2	4	RM	SV	LS	CS
12	3	4	2	1	3	RM	SV	LS	CS
13	4	1	4	2	3	RM	SV	LS	CS
14	4	2	3	1	4	RM	SV	LS	CS
15	4	3	2	4	1	RM	SV	LS	CS
16	4	4	1	3	2	RM	SV	LS	CS
K_1	K_{A1}	K_{B1}	K_{C1}	K_{D1}	K_{E1}				
K_2	K_{A2}	K_{B2}	K_{C2}	K_{D2}	K_{E2}				
K_3	K_{A3}	K_{B3}	K_{C3}	K_{D3}	K_{E3}				
K_4	K_{A4}	K_{B4}	K_{C4}	K_{D4}	K_{E4}				
R	$K_{\max A_i} - K_{\min A_i}$	$K_{\max B_i} - K_{\min B_i}$	$K_{\max C_i} - K_{\min C_i}$	$K_{\max D_i} - K_{\min D_i}$	$K_{\max E_i} - K_{\min E_i}$				

Table 3. Factor level and value.

Factor / Level	A	B	C	D	E
1	0	0	1.2 mm	0.55 mm	0.1 mm
2	2	2	1.5 mm	0.65 mm	0.12 mm
3	−2	4	0.8 mm	0.45 mm	0.08 mm
4	−4	−2	0.6 mm	0.35 mm	0.06 mm

2.3. Material properties

Table 4. Material properties of nitinol alloy and graft.

Nitinol	
Austenite Young's modulus E_A (MPa)	650000
Austenite Poisson's ratio μ_A	0.33
Martensite Young's modulus E_A (MPa)	40000
Martensite Poisson's ratio μ_M	0.33
Transformation strain ε^L	0.041
Loading $\left(\delta\sigma/\delta T\right)_L \left(\mathrm{MPaT^{-1}}\right)$	6.7
Start of transformation loading $\sigma^S{}_L(\mathrm{MPa})$	440
End of transformation loading $\sigma^E{}_L(\mathrm{MPa})$	540
Reference temperature T_0 (°C)	22
Unloading $\left(\delta\sigma/\delta T\right)_U \left(\mathrm{MPaT^{-1}}\right)$	6.7
Start of transformation loading $\sigma^S{}_U(\mathrm{MPa})$	250
End of transformation loading $\sigma^E{}_U(\mathrm{MPa})$	140
Strain limit $\varepsilon_{\max}$	12%
e-PTFE graft	
Young's modulus E (MPa)	55.2
Poisson's ratio μ	0.46
Ultimate strain ε_R	20%

Due to the remarkable super-elasticity, high flexibility, and shape memory effect [23], the self-expanding nitinol stent has been a popular choice in the TEVAR. The nitinol stent can be crimped easily at a low temperature, returning to its predesigned profile after being released from the catheter at the body temperature. The expanded polytetrafluoroethylene (e-PTFE) is a biocompatible, highly nonreactive, and nontoxic polymer. Currently, it is one of the most popular graft materials [21,31]. In this study, a nitinol stent covered with e-PTFE graft was employed, and the main material properties are presented in Table 4. The nitinol material was modeled with a user material subroutine in ABAQUS 6.14 (Simulia, Providence, RI, USA) [23].

2.4. Boundary and loading conditions

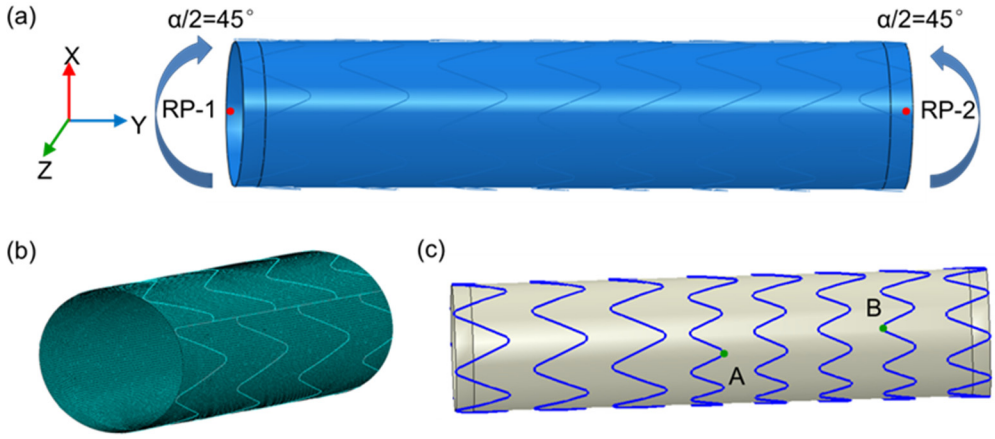

Figure 4. Bending load and element mesh; (a) bending load; (b) element mesh; (c) node pairs.

The FE analyses were undertaken in ABAQUS. The boundary and loading conditions during the analyses are presented in Figure 4a. Both ends of the device were considered as rigid bodies controlled by reference points (RP). The rotations about the *x*-axis and *y*-axis were locked. The translations along *x* and *z* axes were limited at the reference points. During the analysis, the constraint along the *y*-axis was released, and opposite rotations ($\alpha / 2$) were applied on the reference points about the *z*-axis (Figure 4a). To ensure SG's adequate flexibility in the tortuous vessel, the bending angle α here was 90°, which was much higher than the average angle of the aortic arch [33]. The "tie constraint" was employed in ABAQUS to mimic the suture between the metal and graft to prevent sliding and separation during the analyses. The self-contact algorithm was enabled to prevent the self-penetration of the components. As the FE analyses involved high nonlinearities, a dynamic explicit algorithm was employed to prevent non-convergence. The dynamic effect was limited to < 5% of static effects during the analyses [34].

The metal stent was meshed with the 2-nodes beam element (B31), and the graft was meshed with the S4 shell element (Figure 4b). The original model was used to verify the convergence of meshes with five element sizes. The detailed verification is presented in the Supplementary section. Finally, an element size of 0.6 mm was selected because it had acceptable accuracy and lower computing cost. There were approximately 3300 elements in the stent and 45000 elements in the graft.

2.5. Judgment criteria

In this study, the variable geometric parameters' influence on the SG's flexibility and durability was studied. The flexibility study included both global flexibility and local flexibility. A durability study was conducted for both the stent and graft, respectively.

A few assessment criteria have been proposed and applied to the flexibility analyses of SGs with different shapes [10,15]. Some parts of the criteria were adopted and extended to assess the devices' global and local flexibility in this study. The global flexibility reflected the deformability of the stent under the moment and was defined in this study as:

$$\delta = 1/RM$$

where RM was the reaction moment. The higher value of δ indicated better global flexibility. Finally, the global flexibility was assessed by the maximum reaction moment during bending. The global flexibility can be used to reflect the ease of SG transportation within tortuous arteries. After the SG is released within the thoracic aorta, Type II rings are always placed at the aortic arch; hence, adequate local flexibility is required to ensure the sealing effects between the SG and aortic arch.

Local flexibility was first proposed in this study and defined as the spacing variation (SV) along the y-axis between the nodes A and B (Figure 4c). The SV was calculated by the equation:

$$\mathrm{SV} = 1 - L/L_0$$

where L_0 and L are the spaces between the nodes under the un-deformed and deformed states, respectively. A greater SV change reflects better local flexibility.

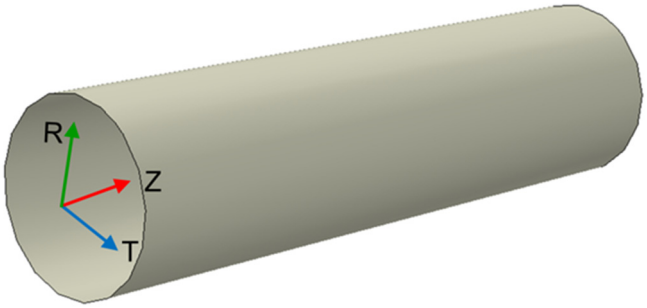

Figure 5. The cylindrical coordinate system.

The durability of the stent and graft was considered respectively during the bending process. The maximum strains of the graft were obtained at both the longitudinal (Figure 5, Z-axial) and circumferential (Figure 5, T-axial) directions during the analyses. Therefore, a cylindrical coordinate system was created to extract the results. The graft's ultimate strains at the longitudinal and circumferential directions were set at 20% equally, and the strain limit of the nitinol alloy was 12% (Table 4).

3. Results

3.1. Device deformation

All the device deformations after bending could be roughly divided into two categories in terms of the deformation shapes: "V" and "U" (Figure 6). The "V" shape was observed in sp6, sp7, sp9, sp10, and sp15, while the "U" shape was seen in the other specimens. In the "V" shape, the graft was folded severely in the middle, where the displacements were also obviously higher than the other positions. Slight wrinkles occurred at the distal and proximal ends of V-shaped specimens. By contrast, the relatively uniformly distributed wrinkles and displacement were found in the "U" shape. The maximum displacements in U-shaped specimens were less than those in V-shaped specimens. Stretching was also observed in the transverse direction of V-shaped specimens. Additionally,

distinct wave shapes associated with the metal wire were observed in the interior aspects of sp4, sp8, sp12, and sp16, which had the least strut numbers. This phenomenon did not occur in other specimens.

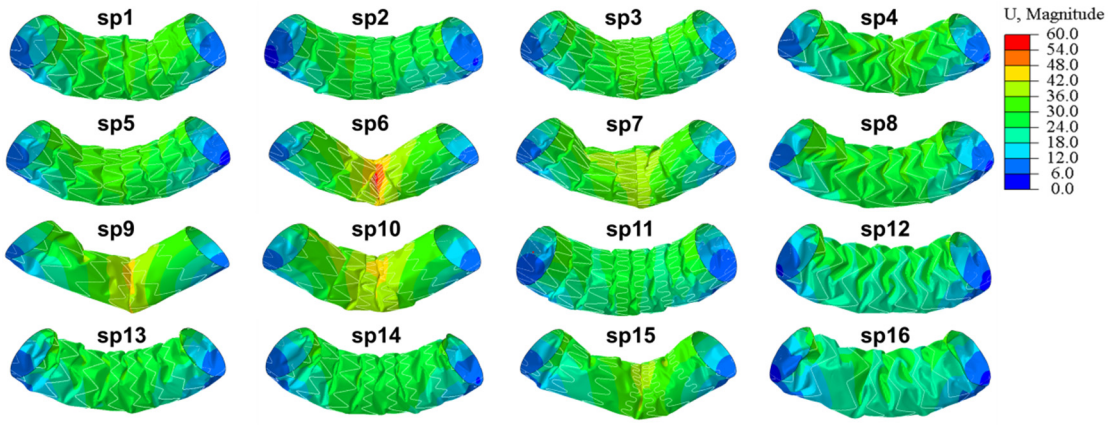

Figure 6. Global deformations of SGs.

3.2. Flexibility

3.2.1. Global flexibility

Figure 7a summarizes the maximum RM values during the bending process. The RM reflected the device's global flexibility directly, and higher RM indicated lower flexibility. In all the models, sp2, sp7, sp8, sp9, sp10, and sp16 exhibited higher values than the sp1, and the other models exhibited lower values. Approximate values, which meant similar global flexibility, were observed in sp4 and sp14; sp5, sp11, sp12, and sp13; and sp6 and sp15, respectively. sp14 and sp4 needed the lowest RM to achieve the predefined shapes while sp2 and sp7 were the most difficult to be bent. The RM of sp7 was more than twice of sp1 and four times of sp14. Hence, sp7 exhibited the lowest flexibility, while sp14 and sp4 were the most flexible models.

Figure 7b-e shows the individual geometric parameters' influences on the maximum RM. The K_i in Figures 7b and 7f monotonically increased in association with increased strut height and graft thickness. Although the K_i fluctuated in Figures 7c and 7e, it tended to be positively related to the increased value of geometric parameters, as shown in Figures 7b and 7f. The strut radius was the only factor to influence K_i inversely. In addition, there were no significant differences in K_i in Figures 7d and 7e, when the strut radius reached 0.8 mm, or the wire diameter reached 0.45 mm. The ranges of K_i obtained from all the factors are presented in Figure 7g. The K_i of graft thickness ranged more widely than those of the other factors, which meant that the graft thickness was the most crucial factor. The strut height was the second most crucial factor in influencing RM. Approximate incidence was obtained from the verified strut number and wire diameter, like from the strut height. The strut radius exerted the slightest effect on RM. Obviously, the importance of factors on RM or global flexibility was E > A > B > D > C in descending order.

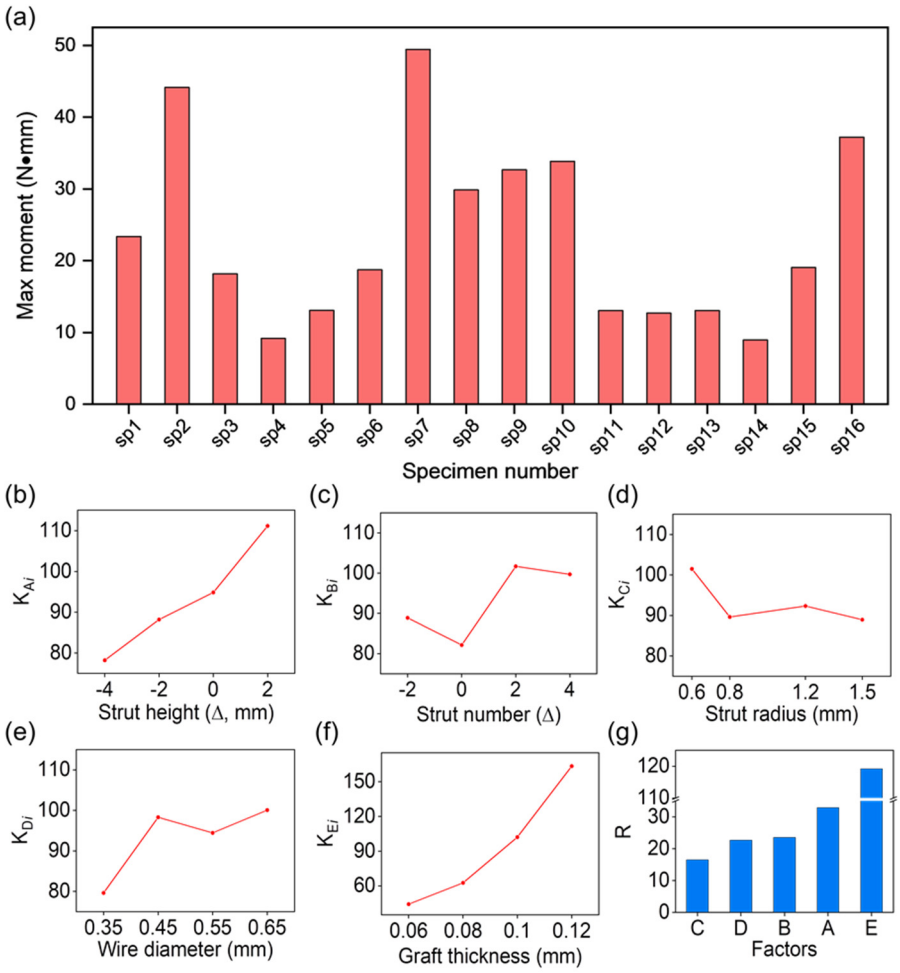

Figure 7. Global flexibility and the analysis of single factors; (a) maximum moments; (b) strut height; (c) strut number; (d) strut radius; (e) wire diameter; (f) graft thickness; and (g) range analysis.

3.2.2. Local flexibility

The device's local flexibility was assessed by the SV of Type II rings, as depicted in Figure 8. The SV in sp9 was the highest in all models, and it was significantly higher than sp1. Specimen16 exhibited the lowest variation, but it was not much lower than sp1, sp11, and sp13; it was close to sp2, sp12, and sp14. In addition, the V-shaped models mentioned in section 3.1 exhibited greater SVs than the other specimens (Figure 8a), and there were no significant differences between them. It presented better local flexibility in V-shaped models than the U-shaped models. In addition to the V-shaped specimens, sp3, sp4, sp5, and sp8 also exhibited higher SV than the original specimen. The SV of sp4 was the highest (approximately 20% higher than sp1) in all the U-shaped models, indicating that sp4 had the best local flexibility.

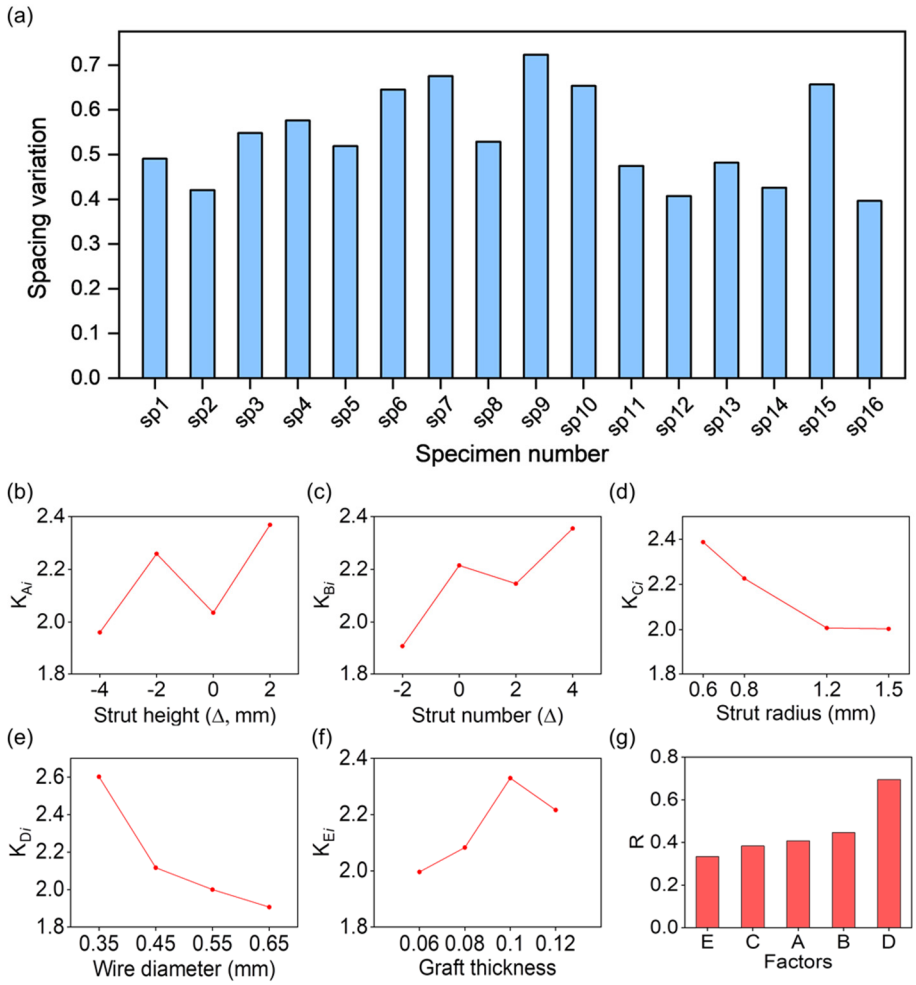

Figure 8. Local flexibility and analysis of a single factor; (a) SVs of Type II rings; (b) strut height; (c) strut number; (d) strut radius; (e) wire diameter; (f) graft thickness; (g) range analysis.

Figure 8b–f lists the influences of a single factor on the local flexibility. Overall, the strut height, strut number, and graft thickness positively impacted the local flexibility; however, there were fluctuations during the process. The K_i decreased rapidly in association with the increased strut radius and wire diameter. The K_i tended to be stable when the strut radius reached 1.2 mm. However, the K_i obtained from the wire diameter continued to decrease. Figure 8g shows the K_i ranges obtained from all the factors. The graft thickness was the weakest factor in influencing local flexibility, contrary to the wire diameter, which significantly influenced local flexibility. There were no significant differences between the ranges obtained from the strut height, strut number, and strut radius. Finally, the local flexibility's critical ranking was: D > B > A > C > E.

3.3. Durability during bending

Figures 9a and 9b separately present the maximum strains in the longitudinal and circumferential directions under a cylindrical coordinate system. Only the circumferential strain of sp7 exceeded the strain limit ε_R, and the others all stayed in a safe range in both directions. The graft

of sp14 exhibited the highest durability for its lowest strains in both directions among all the models. The maximum strain of the metal stent in sp6 was the highest during the bending process. Nevertheless, it was much less than the limit ε_{lim}. The durability of metal stents was not discussed in this study.

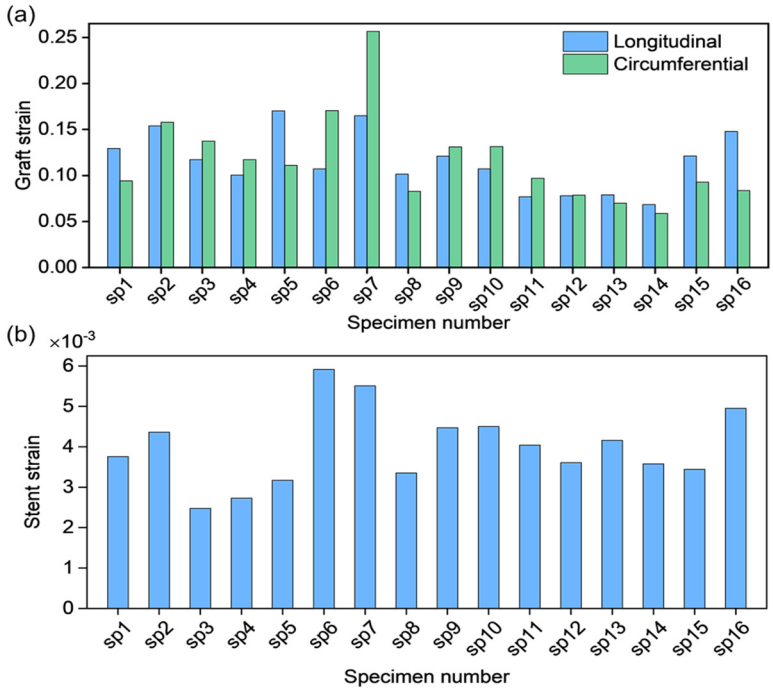

Figure 9. Maximum strains on SG; (a) maximum strains on the graft; and (b) maximum strains on the metal stent.

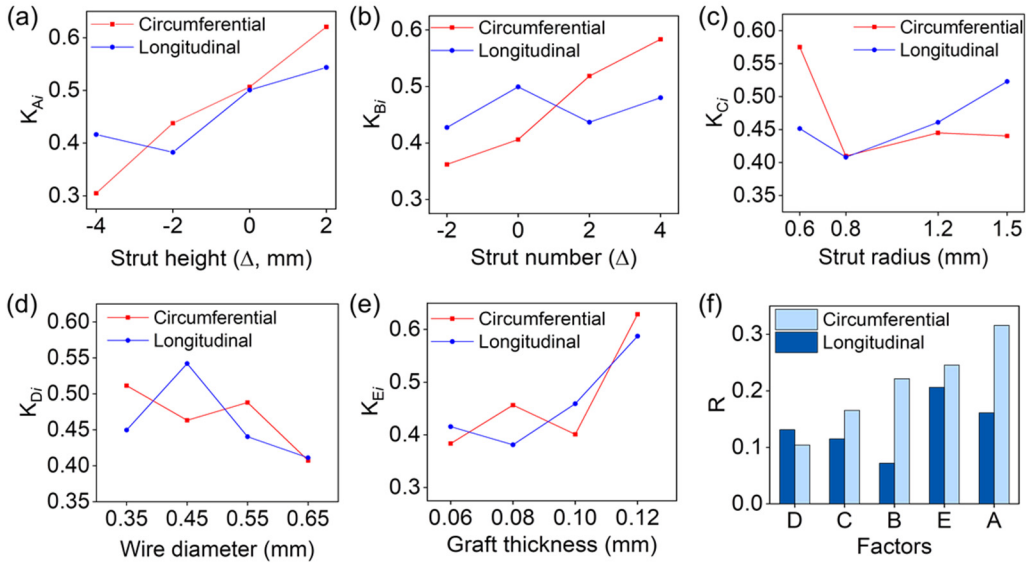

Figure 10. Influences of factors on the local flexibility; (a) strut height; (b) strut number; (c) strut radius; (d) wire diameter; (e) graft thickness; and (f) range analysis.

Figure 10a–e shows the influences on the graft durability of single factors. The factors

positively impacted the circumferential and maximum longitudinal strains, as shown in Figures 10a and 10e. However, the reverse phenomenon occurred in Figure 10d. The maximum strains in both directions decreased with an increase in the wire diameter, indicating an increase in durability. Meanwhile, the maximum circumferential strain increased monotonically with an increase in the strut number while the maximum longitudinal strain fluctuated smoothly within the range (Figure 10b). When the strut radius increased from 0.6 to 0.8 mm, the maximum strains in both directions decreased simultaneously. Then, the maximum circumferential strain changed slightly, and the maximum longitudinal strain increased linearly with the increased strut radius. Figure 10f summarizes the importance of geometric parameters on device durability. The graft thickness exerted the most significant influence on the maximum longitudinal strain, and the strut height influenced the circumferential durability significantly. The factors influencing the circumferential and longitudinal durability in descending order were as follows: A > E > B > C > D and E > A > D > C > B, respectively.

4. Discussions

Improved flexibility might extend the application of SGs in the wide range of anatomical vascular morphology [14,15]. It has been verified that device flexibility is influenced by geometric parameters of the metal stent and graft [29,30]. However, influences on SGs' flexibility, mainly from one or few parameters, had been studied. Here, the thoracic aorta SGs were designed and optimized in terms of the influence of comprehensive geometric parameters on flexibility. The influences of each parameter were obtained, and the important ranking of all the impacting factors was examined. At the same time, the influences on device durability during the bending process were also investigated. Our study's results indicated that these geometric parameters exerted different influences on flexibility and durability, which provides the strategy of designing the thoracic aortic SGs, especially for the thoracic aortic arch diseases.

The thoracic aorta SG selected in this study had a special structure that contained three types of wire rings connected by a lateral bar. Due to the lower bending stiffness, the device was more flexible at the Type II wire rings. Therefore, the SV of Type II rings was proposed as local flexibility, which was analyzed in association with global flexibility.

Here, the significant effect on global flexibility mainly came from the graft properties. Although the other parameters were different among the specimens, a common thread occurred in sp2, sp7, sp9, and sp16; they were covered with the thickest graft and had much higher RM than the other models (Figure 7a). A similar phenomenon also occurred in sp14 and sp4, covered with the thinnest graft, and with the lowest RM. In addition, the graft thickness was confirmed as the most influential factor on global flexibility in terms of range analyses, and its effect surpassed the other factors (Figure 7g). For all metal stent parameters, except the strut radius, their increase brought about lower global flexibility. Partial parameters have been confirmed or reported in previous studies [26, 29]. Among all the models, the sp14 exhibited the most favorable parameters from the graft and the metal stent on improving global flexibility, and it becomes the most flexible device.

Contrary to sp4, sp7 gathered the most impact factors that would reduce global flexibility except for the wire diameter. Although the wire diameter was not the weightiest factor on global flexibility (Figure 7g), the original size of the wire diameter (0.55 mm) induced a higher RM (Figure 7e). Thus, sp7 exhibited the highest RM corresponding with the worst global flexibility.

Distinct "V" shapes and transverse stretches were observed in sp6, sp7, sp9, sp10, and sp15

(Figure 6a), representing drastic shape changes of the cross-section, which were adopted as an assessment criterion for device flexibility [10]. The higher SVs in Figure 8a demonstrated their better local flexibility. The curves had the same trend as in Figures 7b, 7c, 7d, and 7f, and Figure 8b–f; however, they represented the opposite effects on global and local flexibility. The wire diameter was the unique factor that had the same effect on both global and local flexibility. Therefore, it was difficult to achieve the best global and local flexibility in the same specimen. For instance, sp7 had the weakest global flexibility, but it also had almost the best local flexibility in all the models; sp4 had the optimum factor (thinnest graft and the most delicate wire) among all the models for improving global and local flexibility, with better global and local flexibility synchronously. Unlike the global flexibility analyses, the most significant influencing factor was wire diameter, and the weakest factor was the graft thickness in influencing local flexibility (Figure 8g). The importance of strut numbers did not exhibit significant differences in influencing global and local flexibility.

In the current study, the influences of geometrical parameters on the durability of SGs were also summarized, which provides a strategy for designing thoracic aortic SGs. Variations in geometric parameters of SG induced different folding behaviors of graft, as shown in Figure 6. The strains were related to the folding behavior. In other words, the durability of the graft would be influenced by geometric parameters. The maximum circumferential strain in sp7 demonstrated that graft durability should not be neglected. Figure 10f also shows that the most critical impacts on circumferential and longitudinal strains were the strut height and graft thickness, respectively. Variations in the two factors also have the same significant effect on global flexibility (Figure 7g). Therefore, decreased strut height and graft thickness properly leads to increased global flexibility and graft durability.

5. Conclusions

In summary, our results indicated that these geometric parameters exerted different influences on flexibility and durability. An SG with better global flexibility can be easily transmitted in the tortuous vessels, and a device with better local flexibility is more applicable for the thoracic aortic arch disease to avoid endoleak.

Acknowledgments

This work was supported by the China-Singapore Joint Research Program (No. 2016YFE0117200).

Conflict of Interest

The authors declare that they have no competing interests.

References

1. V. S. Ramanath, J. K. Oh, T. M. Sundt, K. A. Eagle, Acute aortic syndromes and thoracic aortic aneurysm, *Mayo Clin. Proc.*, **84** (2009), 465–481.
2. M. S. Makaroun, E. D. Dillavou, G. H. Wheatley, R. P. Cambria, Five-year results of endovascular treatment with the Gore TAG device compared with open repair of thoracic aortic

aneurysms, *J. Vasc. Surg.*, **47** (2008), 912–918.
3. S. R. Walsh, T. Y. Tang, U. Sadat, J. Naik, M. E. Gaunt, R. B. Jonathan, et al., Endovascular stenting versus open surgery for thoracic aortic disease: Systematic review and meta-analysis of perioperative results, *J. Vasc. Surg.*, **47** (2008), 1094–1098.e3.
4. T. Baba, T. Ohki, Y. Kanaoka, K. Maeda, Clinical Outcomes of Left Subclavian Artery Coverage on Morbidity and Mortality During Thoracic Endovascular Aortic Repair for Distal Arch Aneurysms, *World J. Surg.*, **39** (2015), 2812–2822.
5. R. J. Feezor, W. A. Lee, Management of the Left Subclavian Artery during TEVAR, *Semin. Vasc. Surg.*, **22** (2009), 159–164.
6. J. C. Ingrund, F. Nasser, S. G. Jesus-Silva, R. P. Limaco, F. L. Galastri, M. C. Burihan, et al., Hybrid procedures for complex thoracic aortic diseases, *Braz. J. Cardiovasc. Surg.*, **25** (2010), 303–310.
7. H. Wouter, F. J. V. Schlösser, F. L. Moll, B. E. Sumpio, B. E. Muhs, Thoracic endovascular aortic repair with the chimney graft technique, *J. Vasc. Surg.*, **58** (2013), 502–511.
8. C. M. T. Jost, Stenting in Europe, what lessons can we learn? Development of a stent classification system based on a survey of European clinical experiences, *Catheterization Cardiovasc. Interventions*, **45** (1998), 217–232.
9. L. Petrini, F. Migliavacca, F. Auricchio, G. Dubini, Numerical investigation of the intravascular coronary stent flexibility, *J. Biomech.*, **37** (2004), 495–501.
10. N. Demanget, S. Avril, P. Badel, L. Orgéas, C. Geindreau, J. N. Albertini, et al., Computational comparison of the bending behavior of aortic stent-grafts, *J. Mech. Behav. Biomed. Mater.*, **5** (2012), 272–282.
11. C. Alfio, P. L. Faries, N. J. Morrissey, T. Victoria, J. A. Burks, E. C. Gravereaux, et al., Predicting iliac limb occlusions after bifurcated aortic stent grafting: anatomic and device-related causes, *J. Vasc. Surg.*, **36** (2002), 679–684.
12. S. R. Dixon, Stent longitudinal flexibility: A comparison of 13 stent designs before and after balloon expansion, *Catheter Cardiovasc. Intervention*, **50** (2000), 120–124.
13. W. Q. Wang, D. K. Liang, D. Z. Yang, M. Qi, Analysis of the transient expansion behavior and design optimization of coronary stents by finite element method, *J. Biomech.*, **39** (2006), 21–32.
14. F. R. Arko, W. A. Lee, B. B. Hill, P. Cipriano, T. J. Fogarty, C. K. Zarins, Increased Flexibility of AneuRx Stent-Graft Reduces Need for Secondary Intervention following Endovascular Aneurysm Repair, *J. Endovascular Ther.*, **8** (2001), 583–591.
15. N. Demanget, A. Duprey, P. Badel, L. Orgéas, S. Avril, C. Geindreau, et al., Finite element analysis of the mechanical performances of 8 marketed aortic stent-grafts, *J. Endovascular Ther.*, **20** (2013), 523–535.
16. J. N. Albertini, M. A. DeMasi, J. Macierewicz, R. E. Idrissi, B. R. Hopkinson, C. Clement, et al., Aorfix Stent Graft for Abdominal Aortic Aneurysms Reduces the Risk of Proximal Type 1 Endoleak in Angulated Necks: Bench-Test Study, *Vascular*, **13** (2005), 321–326.
17. A. R. Weale, K. Balasubramaniam, J. Hardman, M. Horrocks, Use of the AorfixTM stent graft in patients with tortuous iliac anatomy, *J. Cardiovasc. Surg.*, **51** (2010), 461–466.
18. F. S. Cui, H. P. Lee, C. Lu, P. Chai, Effects of balloon length and compliance on vascular stent expansion, *Int. J. Appl. Mech.*, **2** (2010), 681–697.
19. F. Kabinejadian, F. Cui, B. Su, A. Danpinid, H. Pei, H. L. Leo, Effects of a carotid covered stent with a novel membrane design on the blood flow regime and hemodynamic parameters

distribution at the carotid artery bifurcation, *Med. Biol. Eng. Comput.*, **53** (2015), 165–177.
20. A. Karimi, M. Navidbakhsh, H. Yamada, R. Razaghi, A nonlinear finite element simulation of balloon expandable stent for assessment of plaque vulnerability inside a stenotic artery, *Med. Biol. Eng. Comput.*, **52** (2014), 589–599.
21. C. Kleinstreuer, Z. Li, C. A. Basciano, S. Seelecke, M. A. Farber, Computational mechanics of Nitinol stent grafts, *J. Biomech.*, **41** (2008), 2370–2378.
22. S. D. Bock, F. Iannaccone, G. D. Santis, M. D. Beule, D. V. Loo, D. Devos, et al., Virtual evaluation of stent graft deployment: A validated modeling and simulation study, *J. Mech. Behav. Biomed. Mater.*, **13** (2012), 129–139.
23. G. P. Kumar, F. Cui, A. Danpinid, B. Su, J. K. F. Hon, H. L. Leo, Design and finite element-based fatigue prediction of a new self-expandable percutaneous mitral valve stent, *Comput. Aided Des.*, **45** (2013), 1153–1158.
24. N. Demanget, L. Orgéas, P. Badel, S. Avril, C. Geindreau, J. N. Albertini, et al., Severe Bending of Two Aortic Stent-Grafts: An Experimental and Numerical Mechanical Analysis, *Ann. Biomed. Eng.*, **40** (2012), 2674–2686.
25. K. Mori, T. Saito, Effects of Stent Structure on Stent Flexibility Measurements, *Ann. Biomed. Eng.*, **33** (2005), 733–742.
26. G. P. Kumar, L. Mathew, Self-expanding aortic valve stent-material optimization, *Comput. Biol. Med.*, **42** (2012), 1060–1063.
27. W. Wu, L. Petrini, D. Gastaldi, T. Villa, M. Vedani, E. Lesma, et al., Finite element shape optimization for biodegradable magnesium alloy stents, *Ann. Biomed. Eng.*, **38** (2010), 2829–2840.
28. H. H. Zhang, H. Q. Feng, J. Liu, K. Wang, Simulation on flexibility of vascular stent and grey correlation analysis, *J. Med. Biomech.*, **31** (2016), 206–212.
29. Y. Liu, G. Zhu, H. Yang, C. Wang, P. Zhang, G. Han, Bending behaviors of fully covered biodegradable polydioxanone biliary stent for human body by finite element method, *J. Mech. Behav. Biomed. Mater.*, **77** (2018), 157–163.
30. L. Gu, S. Santra, R. A. Mericle, A. V. Kumar, Finite element analysis of covered microstents, *J. Biomech.*, **38** (2005), 1221–1227.
31. I. C. T. Santos, A. Rodrigues, L. Figueiredo, L. A. Rocha, J. M. R. S. Tavares, Mechanical properties of stent-graft materials, Proceedings of the Institution of Mechanical Engineers Part L *J. Mater. Des. Appl.*, **226** (2012), 330–341.
32. A. Wanhainen, R. Nyman, M. O. Eriksson, First report of a late type III endoleak from fabric tears of a Zenith stent graft, *J. Vasc. Surg.*, **48** (2008), 723–726.
33. I. Y. Shin, Y. G. Chung, W. H. Shin, S. B. Im, B. T. Kim, A Morphometric Study on Cadaveric Aortic Arch and Its Major Branches in 25 Korean Adults: The Perspective of Endovascular Surgery, *J. Korean Neurosurg. Soc.*, **44** (2008), 78–83.
34. H. H. Choi, S. M. Hwang, Y. H. Kang, J. Kim, B. S. Kang, Comparison of Implicit and Explicit Finite-Element Methods for the Hydroforming Process of an Automobile Lower Arm, *Int. J. Adv. Manuf. Technol.*, **20** (2002), 407–413.